RSC Advances

PAPER

View Article Online
View Journal | View Issue

Cite this: *RSC Adv.*, 2020, **10**, 2085

Synthesis of poly(ionic liquid) for trifunctional epoxy resin with simultaneously enhancing the toughness, thermal and dielectric performances

Bingyan Yin,[a] Wenqing Xu,[a] Chengjun Liu,[a] Miqiu Kong, *[a] Yadong Lv,[a] Yajiang Huang,[b] Qi Yang[b] and Guangxian Li[b]

Received 14th December 2019
Accepted 30th December 2019

DOI: 10.1039/c9ra10516f

rsc.li/rsc-advances

Poly(ionic liquid) (PIL), integrating the characteristics of both polymers and ionic liquid, is synthesized and employed to modify diglycidyl-4,5-epoxy-cyclohexane-1,2-dicarboxylate (TDE-85). With the addition of PIL, the fracture toughness, and thermal and dielectric performances of TDE-85 were discovered to be simultaneously improved, meanwhile the tensile modulus and strength is increased. Upon an optimal loading of 3 wt% PIL, the critical stress intensity factor (K_{IC}), tensile modulus and strength are raised by 92.9%, 13.3% and 10.7%, respectively. Multi-toughening mechanisms due to spherical domains of PIL formed in TDE-85 during curing are responsible for the improved toughness. Moreover, the dielectric and thermal properties of TDE-85 are also enhanced by adding PIL. With the optimal addition of 5 wt% PIL, the dielectric constant of the composites is enhanced by 62.5%, the glass transition temperature is increased by 16.58 °C and the residual weight of carbon is increased by 59%.

1. Introduction

Epoxy resins with excellent mechanical properties and superior process ability have extensively served as coating products, adhesive materials, electronic encapsulates and structural materials in industries. However, the structure of epoxy resins with high crosslink density limits the movement of molecular chains, which makes them have intrinsic brittleness. Therefore, it is a key task to ameliorate the fracture toughness of epoxy resins to meet the requirements for industrial application.

Up to now, one of most common methods to ameliorate the fracture resistance of epoxy resin is introducing another phase, such as rubber elastomers,[1–5] thermoplastics,[6–8] block copolymers[9–15] and nanofillers,[16–22] into the epoxy resin. Through these methods, toughened epoxy resins are indeed achieved but mostly at the expense of deterioration in thermal resistance, which limits their applications. The origins of the degraded thermal properties are closely related to kinds of polymers used to toughen. Therefore, to find a relatively appropriate polymer for simultaneously improving the toughness and thermal properties for epoxy resins is important in science, which possesses a profound prospect in industrial applications.

PIL, integrating the characteristics of both polymers and ionic liquid (IL), presents high ionic conductivities, wider electrochemical windows, high thermal stabilities, nonflammability and good compatibility.[23–27] Actually, studies on the functional properties of PIL used as solid ionic conductors or dielectric properties,[28–31] powerful dispersant and stabilizer,[32] absorbent,[33,34] porous polymer[35–37] have been extensively reported; while there are relatively few studies dealing with the influences of PIL on the mechanical and functional properties of other polymers. It is reported that introducing PIL can prominently enhance the toughness, tensile strength, dielectric properties and thermal performance of polymers, but focused on the hyper branched polymeric ionic liquids (HPILs)[38–40] and PIL used as modifier for carbon fillers.[41–43] For instance, Zhang *et al.*[38] found that the cross linking reaction between diglycidyl ether of bisphenol A (DGEBA) and methylhexahydrophthalic anhydride (MHHPA) is accelerated by a hyper branched ionic liquid (HBP-Mim), and the impact, tensile and flexural strength are significantly improved by 131.0%, 63.1% and 135.2% in the presence of 9 phr HBP-Mim, respectively. Chen *et al.*[40] showed that, for benzoxazine/epoxy composites, the curing temperature is remarkably lowered by the introduction of HPILs (HBP-[AMIM][PF_6]) meanwhile the mechanical and thermal performances are improved. Moreover, PIL can be used as an effective dispersant or interfacial modifier of graphene[42,43] and nanotube[41] in the polymer matrix, which can enhance the dispersion of nanoparticles and thus improve the properties of composites. For instance, the dielectric loss for cyanate ester (CE)/graphene is reduced when the surfaces of graphene are coated by PIL, which is due to PIL coated on graphene act as electron insulative layers which induces the leakage current between conductive carbon layers.[42] However, effects of PIL on the

[a]School of Aeronautics and Astronautics, Sichuan University, Chengdu 610065, People's Republic of China. E-mail: miqiukong@scu.edu.cn

[b]College of Polymer Science and Engineering, State Key Laboratory of Polymer Materials Engineering of China, Sichuan University, Chengdu 610065, People's Republic of China

comprehensive performances in particular mechanical, thermal and dielectric performances of epoxy resins have still unveiled yet.

In this work, PIL (P[BVIM][BF_4]) is synthesized from IL and utilized to modify the comprehensive properties of the trifunctional epoxy resin (TDE-85). Effects of different concentrations (0–5 wt%) of PIL on the mechanical performance, thermal capacity and dielectric properties of TDE-85 are systematically explored. It is shown that the fracture resistance of epoxy/PIL composites is significantly raised meanwhile the thermal and dielectric properties are enhanced by introducing PIL. And the toughening mechanisms of TDE-85 modified by PIL are debated.

2. Experimental

2.1 Materials

The trifunctional diglycidyl 4,5-epoxyhexane-1,2-dicarboxylic acid ester epoxy resin (TDE-85) was used (Tianjin Institute of Synthetic Materials Industry, China). The epoxy value of TDE-85 is 0.85The 4,4-diaminodiphenylmethane (DDM, 98%) (Huayi Resin, Shanghai, China) was employed as the hardener. 1-Butyl-3-vinylimidazole tetrafluoroborate ([BVIM][BF_4], 99%) ionic liquid was obtained from Shanghai Chengjie Chemical Co., Ltd (China) and always preserved in a desiccator containing silica gel to prevent from atmospheric moisture. Acetone (analytical purity) was provided by Changlian Chemical Reagent Co., Ltd, Chengdu. Ethanol (analytical purity) and azobis(isobutyronitrile) (AIBN) from Aladdin was employed as the initiator. Before use, AIBN was recrystallized and purified in methanol, while other substances were applied as received. Fig. 1 displays the molecular structures of trifunctional epoxy resin (TDE-85), hardener (DDM) and ionic liquid monomer ([BVIM][BF_4]).

2.2 Polymerization of PIL

PIL was synthesized from the ionic liquid (IL) through bulk polymerization. The polymerization process of PIL is schemed in Fig. 2. Firstly, 29.89 g of ionic liquid monomer ([BVIM][BF_4]) was added into the reaction bottle and then degassed by using a vacuum pump for 5 min at ambient temperature. Next, purified AIBN (0.11 g) was put into the reaction bottle in the water bath at 40 °C and stirred until AIBN was dissolved completely. Again, the system was degassed under vacuum, and nitrogen gas was injected to ensure that the system kept anaerobic. After that, the mixed solution reacted in water bath at 65 °C for 5 hours until it became completely solid, and the obtained solids were dissolved in acetone and purified by precipitation in ethanol. Then, the obtained products were placed at ambient temperature for at least 48 hours to remove the solvent and then placed in vacuum oven under 80 °C for a day and night. Finally, the yield of PIL (P[BVIM][BF_4]) can be referred as the ratio of the weight for the purified PIL and the ionic liquid monomers used in the polymerization, which was calculated to be about 60.3%.

2.3 Preparation of epoxy/PIL composites

As shown in Fig. 2, 40 g TDE-85 and 16.7 g DDM were firstly mixed in a conical flask (100 ml) and stirred in water bath at 60 °C until DDM was completely dissolved. Next, various amounts (1 wt%, 3 wt% and 5 wt%) of PIL were dissolved in 15 ml acetone, respectively, and then the obtained solution was mixed with TDE-85/DDM mixture and stirred uniformly. After that, the mixture of TDE-85/DDM was decanted into the preheated polytetrafluoroethylene molds and the solvent was volatilized at ambient temperature for at least 48 hours. Finally, the mold was placed the oven and the curing process was set as 80 °C for 2 h and 120 °C for another 2 h. After the completion of curing, samples were released from the mold after slowly cooled down near to ambient temperature.

2.4 Characterizations

The changes of molecular structures between IL and PIL were characterized by employing a Fourier transform infrared spectrometer (Nicolet 6700, Thermo Fisher Scientific, USA). The spectra was conducted in a transmission mode with a resolution 4 cm^{-1} and 32 scans were done in a wavelength range from 4000 cm^{-1} to 650 cm^{-1}. Before testing, IL was coated on potassium bromide window and PIL was mixed with potassium bromide and pressed into flakes.

To determine the microstructure state of the PIL, two-dimensional wide-angle X-ray diffraction (XRD) was fulfilled in the range of $2\theta = 5–60°$ ($2° \ min^{-1}$) by using Philips X' Pert PRO with Cu-Kα radiation at 40 kV and 40 mA. The wavelength used was 0.124 nm.

To study the molecular weight and polydispersity index of PIL, the measurements of gel permeation chromatography (GPC) were performed on a Waters 1525 (Agilent PL gel 5 μm MIXED-C) from Waters Corporation. Dimethyl formamide (DMF) with added $NaBF_4$ (0.11 g L^{-1}) was employed as the eluent at a flow rate of 1.0 ml min^{-1}, and mono-dispersed polystyrene was used as the calibration standards.

To elucidate the molecular structure of PIL, the spectra of ^1H NMR (400 MHz) were conducted with a Bruker spectrometer

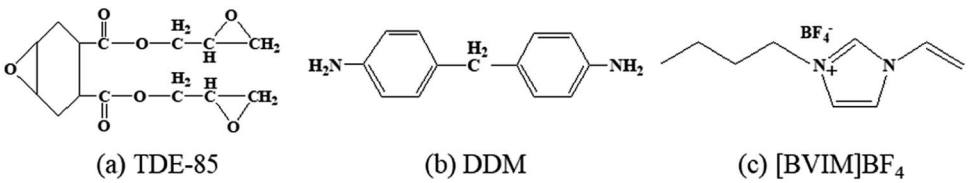

Fig. 1 Molecular structures of substances: (a) diglycidyl 4,5-epoxyhexane-1,2-dicarboxylic acid ester (TDE-85), (b) hardener (DDM) and (c) ionic liquid monomer ([BVIM][BF_4]).

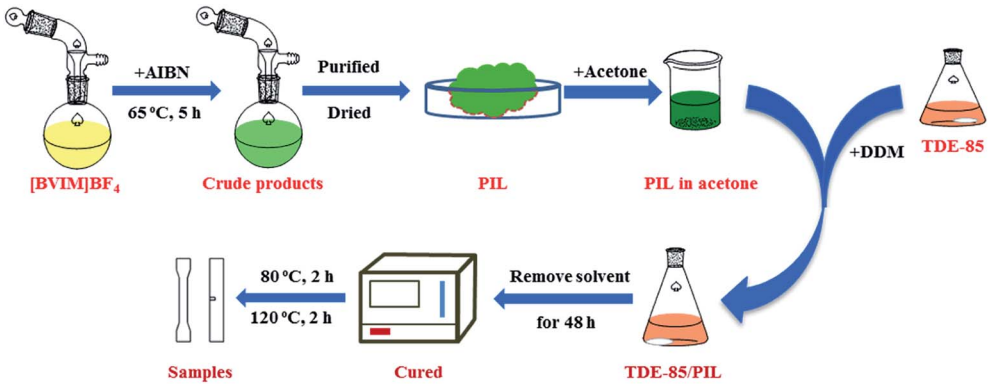

Fig. 2 Preparation of PIL and TDE-85/PIL composites.

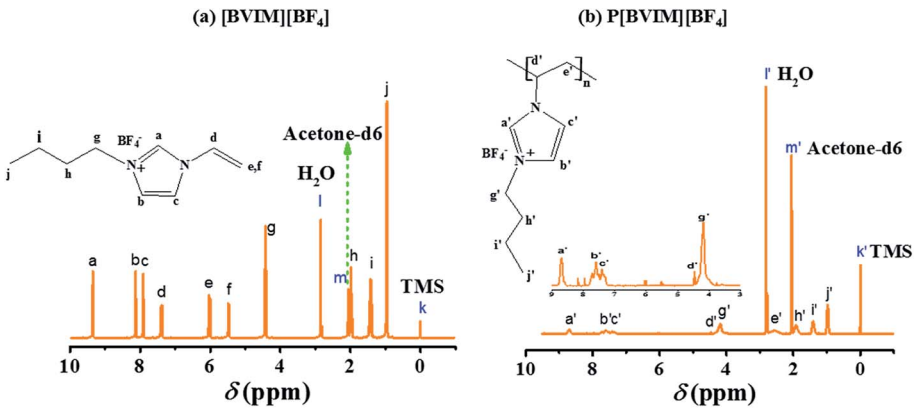

Fig. 3 ^{1}H NMR spectrum of (a) IL and (b) PIL. Inset in (a) represents the molecular structure of IL, in which the assignments of signals for IL are labeled in alphabet a to m. Insets in (b) represent the molecular structure of PIL (the assignments of signals for PIL are labeled in alphabet a′ to m′) and the enlargements of signals from δ 3.00 ppm to δ 9.00 ppm, respectively.

(Avance III, Germany). Deuterated acetone (C_3D_6O) and tetramethysilane are used as the solvent and internal standard, respectively.

The curing behavior of TDE-85/PIL composites was probed by a differential scanning calorimeter (DSC, Q250, TA, USA) in nitrogen atmosphere. After uniformly mixing the composites,

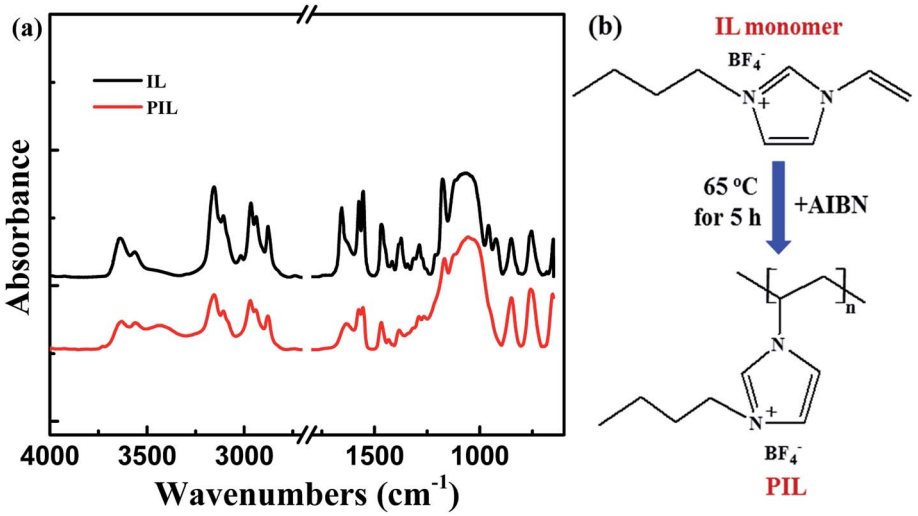

Fig. 4 (a) The spectra of FTIR for IL ([BVIM][BF_4]) and PIL (P[BVIM][BF_4]) and (b) scheme for the chemical reactions from IL monomer to PIL.

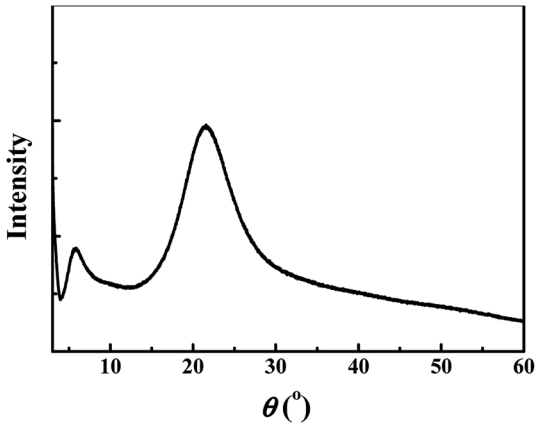

Fig. 5 XRD patterns of PIL.

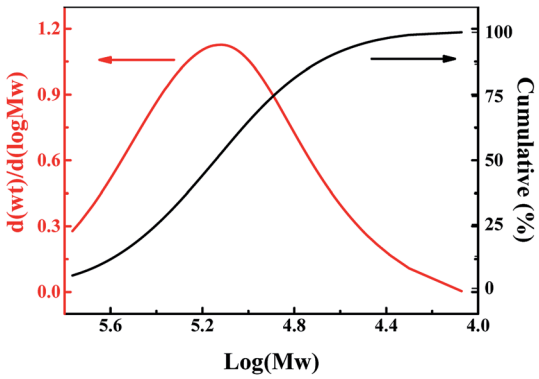

Fig. 6 GPC analysis of PIL.

samples with approximately 5–8 mg were weighted for this measurements. With the velocity of 5 °C min^{-1}, samples were heated from 40 to 350 °C.

Dynamic mechanical analysis (DMA) of the cured TDE-85/PIL composites was conducted on a DMA200 (TA instruments, USA) with a dual cantilever mode at a constant frequency (1 Hz). The temperature is increased from 30 to 300 °C at a speed of 3 °C min^{-1}. The sample dimensions for DMA measurements were 20.0 × 10.0 × 5.0 mm^3.

The mechanical performance of TDE-85/PIL composites were explored by using a 5567 universal testing machine (Instron, USA). Tensile tests were performed with a load cell of 30 kN at a loading speed of 5 mm min^{-1}. Samples for this measurement were prepared according to the standard (ASTM D638-2003) and at least 5 samples were done for each test. Fracture toughness of composites were surveyed with crack-opening tests with the bending rate of 10 mm min^{-1}. In accordance with standard (ASTM D5045-99), samples with dimensions of 44 × 10 × 5 mm^3 were prepared. Before measurements, a sharp razor blade was slided into the notch to trigger a precrack. The results were obtained from the average of at least 8 samples.

The microstructure of TDE-85/PIL composites was characterized by scanning electron microscopy (SEM, FEI Inspect F50) manipulated at 20 kV. Before SEM observation, fractured surfaces of samples were sputtered with gold. The size of PIL phase in epoxy matrix was measured from SEM images by using a home-developed software (imlViewer.exe). At least 200 droplets were analyzed for each sample. The volume-averaged radius (R_v) of PIL droplets were calculated by $R_v = \frac{\sum_i^n (N_v)_i R_i^4}{\sum_i^n (N_v)_i R_i^3}$, in which $(N_v)_i$ is the number of droplets having the radius R_i.

Thermo gravimetric analysis (TGA) was applied to characterize thermal stabilities of composites by using TG209 from NETZSCH Company (Germany) in nitrogen atmosphere. For each sample, about 4–8 mg were weighted and the temperature was elevated from 30 to 800 °C at a velocity of 10 °C min^{-1}.

The dielectric properties of composites were measured by Novocontrol Concept 50 (Germany). The diameter of each sample was 20 mm, and the test frequency was from 1 to 10^7 Hz.

3. Results and discussion

3.1 Characterization of PIL

Fig. 3 reveals the spectra of ^{1}H NMR for IL and PIL, respectively. For the IL (Fig. 3a), the signals of imidazole ring (–N=CH–N–, –N–CH=CH–N– and =N–CH=CH–N–) are obtained at δ 9.35 ppm (a), δ 8.13 ppm (b) and δ 7.91 ppm (c), respectively. The vinyl protons (CH_2=CH–, CH_2=CH– and CH_2=CH–) are

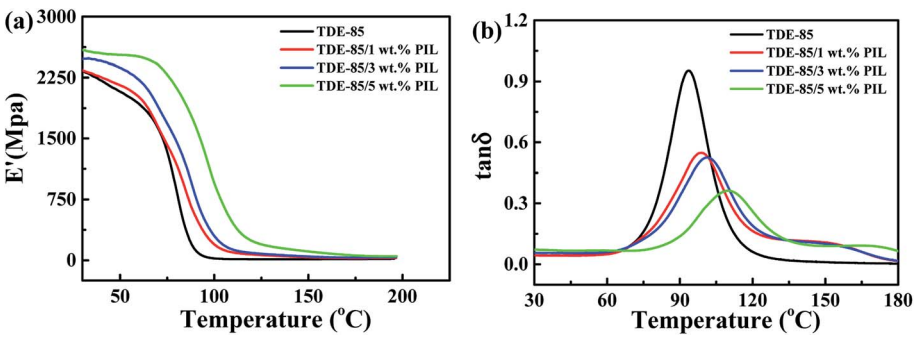

Fig. 7 Thermomechanical properties of TDE-85/PIL composites with the addition of different concentrations (0, 1, 3 and 5 wt%) of PIL: (a) storage modulus (E') as a function of temperature and (b) loss factor (tan δ) as a function of temperature.

Table 1 Storage modulus (E') at the glassy region and rubbery plateau region, glass transition temperature (T_g) and crosslinking density (ρ) of neat epoxy (TDE-85) and epoxy with the addition of different concentrations (0, 1, 3 and 5 wt%) of PIL

	Storage modulus (MPa)			
Compositions	Glassy region	Rubbery region (T_g + 30 °C)	T_g (°C)	ρ (1×10^{-3} mol m^{-3})
TDE-85	2336	12.37	93.51	1.24
TDE-85/1 wt% PIL	2340	59.14	98.76	5.90
TDE-85/3 wt% PIL	2481	70.68	101.25	7.01
TDE-85/5 wt% PIL	2587	135.96	110.09	13.20

obtained at δ 7.39 ppm (d), δ 6.02 ppm (e) and δ 5.47 ppm (f), respectively.[24,44] The peaks at δ 4.42 ppm (g, –NCH_2CH_2–), δ 2.04–1.92 ppm (h, –NCH_2CH_2–), δ 1.42 ppm (i, –NCH_2CH_2-CH_2–) and δ 0.96 ppm (j, –$NCH_2CH_2CH_2CH_3$) are originated from butyl alkyl chain.[44] Note that the peak at δ 2.05 ppm (m) is originated from acetone-d_6 and the peak at δ 2.82 ppm (l) is corresponding to the residual water in IL. For the PIL (Fig. 3b), the peaks at δ 8.70 ppm (a′), δ 7.56 ppm (b′) and δ 7.42 ppm (c′) are corresponding to the protons of imidazole ring, while the signals of the alkyl chain appear at δ 4.19 ppm (g′), δ 1.93 ppm (h′), δ 1.41 ppm (i′) and δ 0.97 ppm (j′). After polymerization of IL into PIL, the peaks at δ 4.45 ppm (d′), δ 2.57 ppm (h′), standing for the proton in the main-chain of PIL, appear, while the peaks of unsaturated vinyl group (CH_2=CH–, δ 7.39 ppm, δ 6.02 ppm and δ 5.47 ppm) disappear, confirming that the complete polymerization of IL monomers into PIL.[24,38,45]

Fig. 4a reveals the spectra of FTIR for IL monomer ([BVIM][BF_4]) and PIL (P[BVIM][BF_4]). It is found that, for IL, absorption peaks located at 3015 cm^{-1} and 952, 922 cm^{-1} are ascribed to the stretching vibration of unsaturated C–H and out-of-plane bending vibration for vinyl, respectively.[44] And absorption peaks at 1650 cm^{-1} and 1060 cm^{-1} can be ascribed to stretching vibration of unsaturated C=C and stretching vibration absorption peak of B–F, respectively. After the polymerization of PIL from IL, absorption peaks representing the stretching vibration of unsaturated C–H (3015 cm^{-1}) and out-of-plane bending vibration (952 cm^{-1} and 922 cm^{-1}) in vinyl disappear. And the stretching vibration peak of C=C (1650 cm^{-1}) is significantly decreased. Note that the stretching vibration peak of residual double carbon bond is attributed to the unsaturated double carbon bond in imidazole rings. These results indicate that the ionic liquid monomer is polymerized completely into PIL,[44,45] and the as shown in Fig. 4b.

Furthermore, as shown in Fig. 5, XRD analysis reveals that PIL is amorphous, which is verified by the broad rather than sharp peak. Moreover, Fig. 6 displays the molecular weight of PIL investigated by GPC. It is displayed that the average number- and weight-molecular weight are 92 300 and 160 000, respectively, and the distribution index of the molecular weight is 1.815.

3.2 Thermomechanical performances of epoxy/PIL composites

Fig. 7 illustrates the thermomechanical performances of epoxy/PIL composites with different concentrations (0, 1, 3 and 5 wt%) of PIL. It shows that the storage modulus (E') of epoxy/PIL composites at low temperatures (the glassy region) is increased with increasing concentration of PIL (Fig. 7a). With further increasing the temperature (T), the E' of epoxy/PIL composites is sharply reduced, which is defined as the

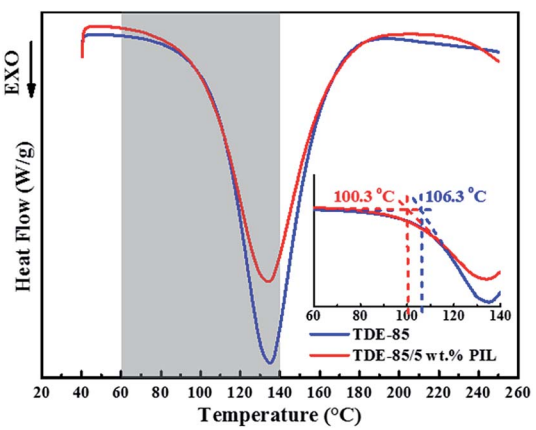

Fig. 8 Curing behavior of pure epoxy (TDE-85) and epoxy/5 wt% PIL composites with the speed of 5 °C min^{-1}. The inset picture is the partial enlargement of the grey part in the figure.

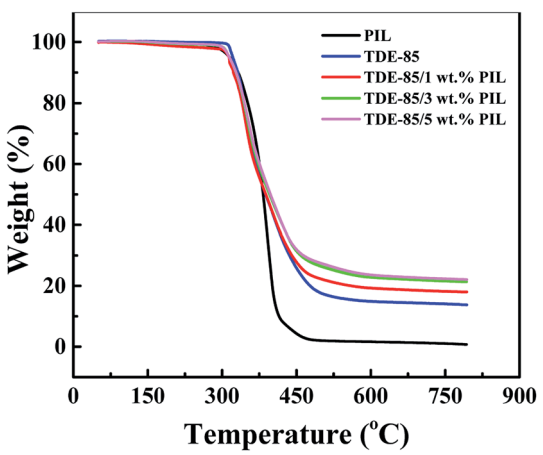

Fig. 9 TGA curves of PIL and epoxy (TDE-85)/PIL composites with different concentrations (0, 1, 3 and 5 wt%) of PIL.

Table 2 The onset degradation temperatures (T_{onset}) and mass of carbon residue at 750 °C of PIL and epoxy/PIL composites with different concentrations (0, 1, 3 and 5 wt%) of PIL

Compositions	T_{onset} (°C)	Carbon residue at 750 °C
PIL	314.5	1.03
TDE-85	321.5	14.08
TDE-85/1 wt% PIL	314.0	18.21
TDE-85/3 wt% PIL	314.5	21.58
TDE-85/5 wt% PIL	314.5	22.35

transition region. Correspondingly, a peak is displayed on the curves of loss tangent (tan δ) *versus* T (Fig. 7b). Generally, the T at the peak is defined as the glass transition temperature (T_g), which is representative of the thermal resistance of composites.[46] Table 1 lists the T_g of epoxy/PIL composites. It is shown that the T_g of epoxy/PIL composites is increased with the increment of the concentration of PIL. Especially when the concentration of PIL is 5 wt%, the T_g of epoxy/PIL composites is increased by 16.58 °C in contrast with that of the neat epoxy resin (93.51 °C). This may be attributed to a more complete network of epoxy/PIL composites in comparison with the neat epoxy resin. It is reported that IL with different cations and anions can be used as curing agent and curing catalyst which can promote the cross-linking of epoxy resin.[47–51] As shown in Fig. 8, the initial curing temperature is decreased by the introduction of PIL due to the promoted curing reaction of epoxy/PIL composites induced by PIL, making local network more complete and thus enhanced the glass transition temperature.

Furthermore, on the basis of the rubbery elasticity of E', the crosslinking density (ρ) of epoxy/PIL composites can be obtained:[52]

$$\rho = \frac{E'}{3RT} \quad (1)$$

in which E' (MPa) denotes the storage modulus of samples at T_g + 30 °C, ρ (mol m^{-3}) denotes cross-linking density, R (J (mol K)$^{-1}$) is the constant of ideal gas, and T (K) represents the absolute temperature at T_g + 30 °C. Then, based on eqn (1), Table 1 shows, the cross-linking density of epoxy/PIL composites. It is seen that the ρ of epoxy/PIL composites is markedly improved with increasing the concentration of PIL. Especially when the concentration of PIL is 5 wt%, the cross-linking density of epoxy/PIL composites (13.20) is increased by about 10 times as compared to 1.24 for the neat epoxy resin. It demonstrates that the introduction of PIL can extremely promote the curing reaction of epoxy resin to make a more complete network. As a consequence, the crosslinking density of epoxy/PIL composites is remarkably improved.

3.3 Thermal behavior of epoxy/PIL composites

Fig. 9 shows the thermal gravimetric curves of PIL, neat epoxy resin and epoxy/PIL composites. Correspondingly, the onset

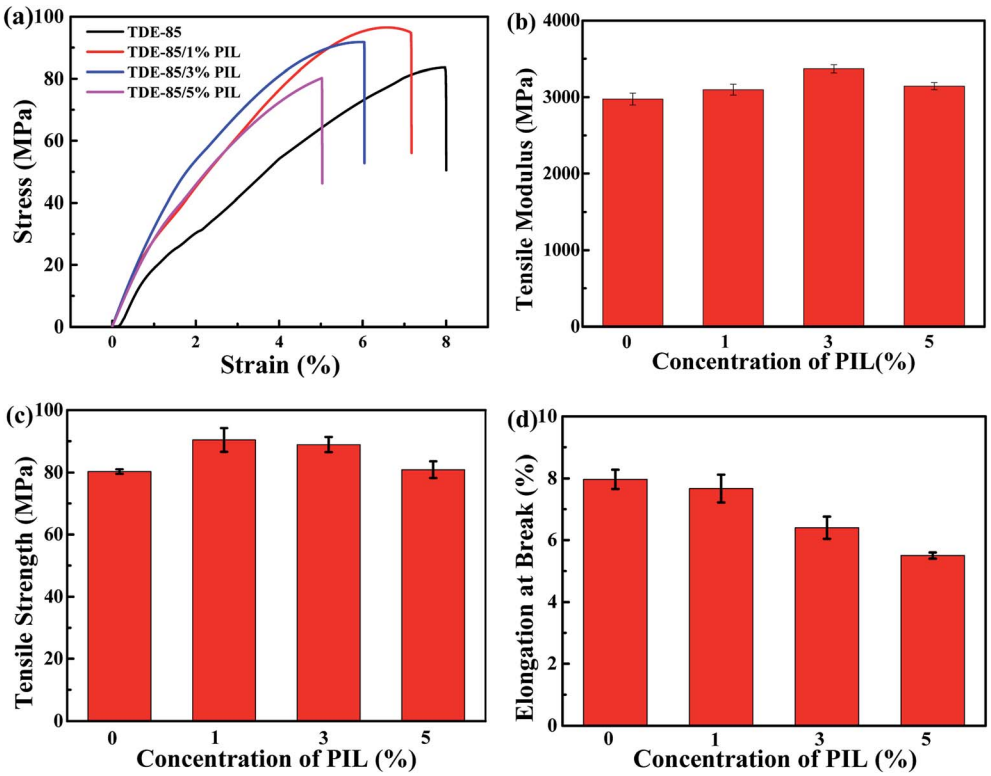

Fig. 10 The mechanical performances of epoxy/PIL composites with different concentrations (0, 1, 3 and 5 wt%) of PIL: engineering stress–strain curves (a); tensile modulus (b), tensile strength (c) and elongation at break (d) as function of PIL concentration.

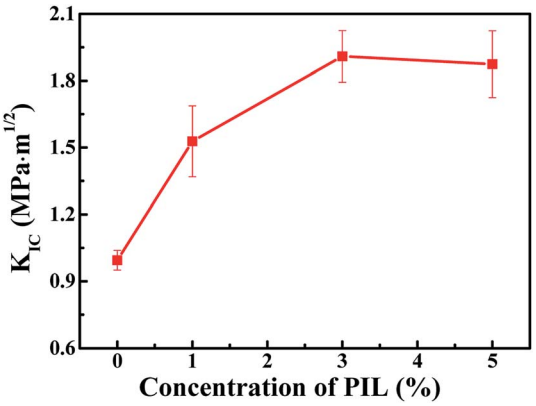

Fig. 11 Fracture toughness (K_{IC}) of TDE-85/PIL composites with different concentrations (0, 1, 3 and 5 wt%) of PIL.

degradation temperatures at 5% weight loss (T_{onset}) and mass of carbon residue at 750 °C are present in Table 2. It is clearly demonstrated that the T_{onset} of epoxy/PIL composites is similar to that of PIL, decreased by about 7 °C as compared to the pure epoxy, meaning that T_{onset} depends on the decomposition of PIL. However, the residual mass at 750 °C of epoxy/PIL composites is increased obviously with the increase of PIL concentration. For the pure PIL and epoxy, the residual mass is only 1.03% and 14.08%, respectively. When 5 wt% of PIL is added, the residual weight is increased to 22.35%, which is improved by 59% in comparison with the neat epoxy. This is because the network of epoxy is promoted to be more complete by the PIL,[53] thereby resulting in the increase of the residual mass.

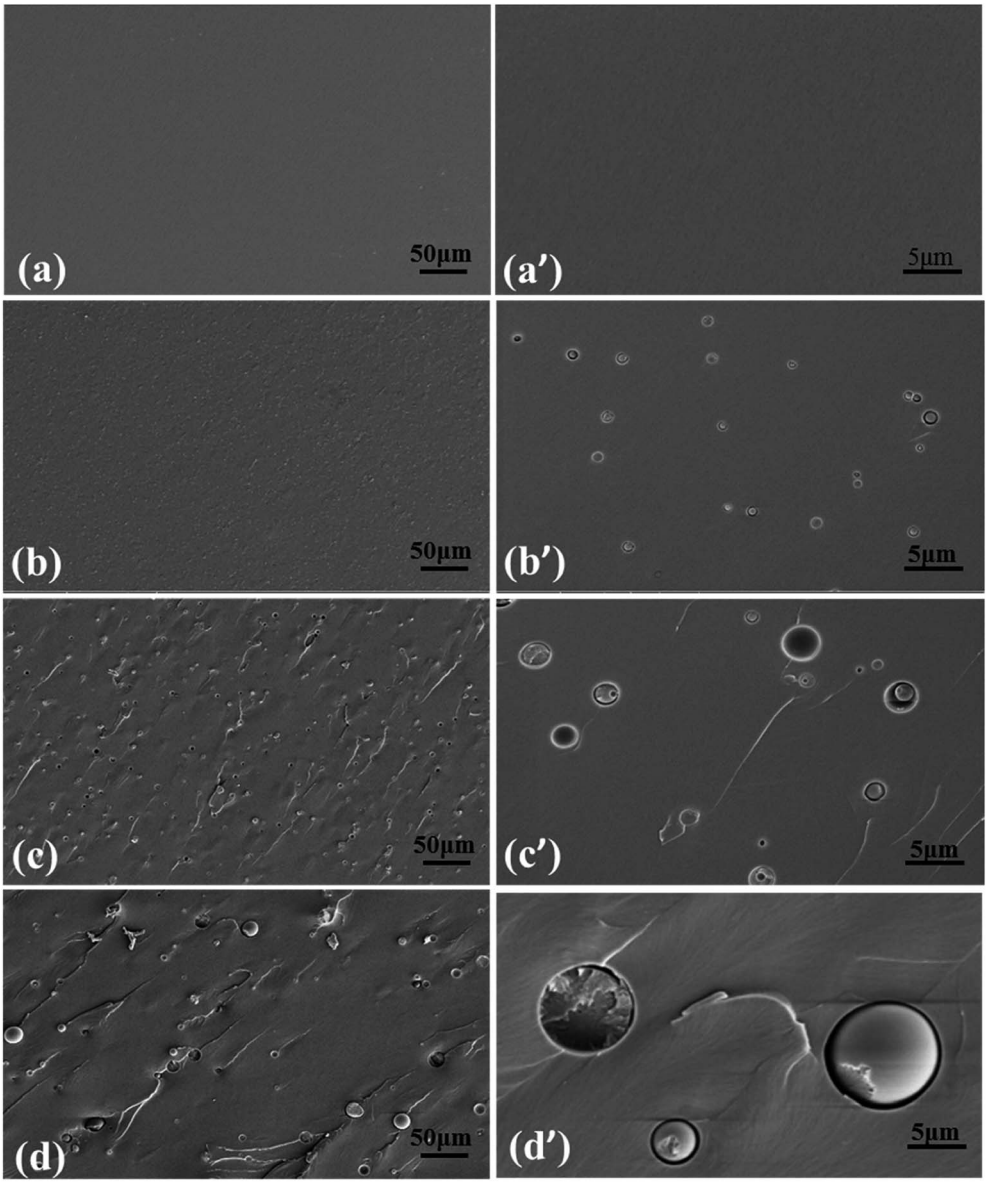

Fig. 12 SEM images showing fracture surfaces of TDE-85/PIL composites with the addition of 0 wt% (a), 1 wt% (b), 3 wt% (c) and 5 wt% (d) of PIL, respectively. (a′)–(d′) are the partial enlargement of the corresponding fracture surfaces (a)–(d), respectively.

3.4 Mechanical performance of epoxy/PIL composites and toughening mechanism

The mechanical performances of epoxy/PIL composites with different concentrations (0, 1, 3 and 5 wt%) of PIL were investigated, as shown in Fig. 10. Representative engineering stress–strain curves for epoxy/PIL composites are plotted in Fig. 10a. Fig. 10b and c illustrates the average values of tensile modulus, tensile strength and elongation at break of epoxy/PIL composites. It is found that the tensile modulus and tensile strength of epoxy/PIL composites are enhanced first and then reduced with the increment the concentration of PIL, but it is always higher than the pure epoxy. When the concentration of PIL is 3 wt%, the tensile modulus and tensile strength of composites are raised to 3369.9 MPa and 88.9 MPa, which is raised by 13.3% and 10.7% in contrast with the neat epoxy, respectively. Moreover, the elongation at break of epoxy/PIL composites is reduced with the increment of the PIL concentration (Fig. 10c). It can be attributed to the increased crosslinking density induced by the promoted curing process of epoxy network by PIL, which is certified by DMA results (Fig. 7).

Moreover, the fracture toughness (K_{IC}) can be characterized by three-point bending tests, which can be calculated by:[54]

$$K_{IC} = \left(\frac{P}{BW^{\frac{1}{2}}}\right) f(x) \quad (2)$$

where $0 < x < 1$,

$$x = a/W \quad (3)$$

$$f(x) = 6x^{1/2}\frac{[1.99 - x(1-x)(2.15 - 3.93x + 2.7x^2)]}{(1+2x)(1-x)^{3/2}} \quad (4)$$

where P represents the maximum load at the three-point bending test; B represents the width of samples and W denotes their thickness; and a represents the length of the crack (including the prefabricated notch length). Based on eqn (2)–(4), the fracture toughness of epoxy/PIL composites is obtained and described in Fig. 11. It is found that, with the introduction of PIL, the fracture resistance of epoxy/PIL composites is significantly boosted. The optimum fracture toughness is 1.91 ± 0.06% MPa $m^{1/2}$ epoxy/3 wt% PIL composites, which is increased by 92.9% as compared to 0.99 ± 0.44% MPa $m^{1/2}$ for the pure epoxy. It indicates that, with the introduction of PIL, the fracture resistance of epoxy resin can be effectively advanced meanwhile the modulus and strength are also increased.

In order to thoroughly elucidate the mechanisms of PIL toughened epoxy resin, Fig. 12 displays the surfaces of fractured epoxy/PIL composites obtained from the tests of three-point bending. For the pure epoxy resin, a smooth cross section exhibits (Fig. 12a), signifying a fracture behavior of typical brittleness. With the introduction of PIL, the fracture surfaces of epoxy/PIL composites become rough and show a droplet/matrix morphology (Fig. 12b–d). And the size of microspheres is increased with the increment of the concentration of PIL, as shown in Fig. 13. When adding 1 wt% PIL, the size of PIL droplets is only about 0.78 μm. With increasing the concentration of PIL up to more than 3 wt%, the dimension of PIL droplets is increased to 2.35 for TDE-85/3 wt% PIL and 8.85 μm for TDE-85/5 wt% PIL, respectively. It was reported that toughening mechanisms of modified epoxy with a droplet/matrix morphology are affected by the droplet size, showing that droplets with smaller size can cause cavitation, whereas droplets with larger size can lead to crack deflection and blockage.[55] During the crack propagation, different toughening mechanisms are triggered in epoxy/PIL composites with different concentrations of PIL. In the composite with low concentration (1 wt%) of PIL, PIL droplets are observed to be completely debonded from the epoxy matrix and the detached PIL droplets are smaller than the holes that host the droplets (Fig. 12b and b′), indicating that shear yielding of matrix around the droplets is happened during crack propagation.[56] Thus, the toughening mechanisms for the composite with low concentration (1 wt%) of PIL are dominated by the debonding of PIL droplets and shear yielding of matrix. For composites with high concentrations (3 and 5 wt%) of PIL, some droplets are also completely debonded from the epoxy matrix (Fig. 12c, c′ and d, d′), which subsequently induces shear yielding of matrix. And some PIL droplets are fractured (Fig. 12c, c′ and d, d′), indicating that cracks cross the PIL droplets, in which PIL droplets can act as obstacles and dissipate energy during the crack propagation.[57] Moreover, some parabolic and elliptical markings are observed on the surfaces of fractured TDE-85/PIL composites (Fig. 12c, c′ and d, d′), which can make the cracks deflection during crack propagation.[46] Furthermore, the presence of PIL droplets can perturb the formation of epoxy network structure and initiate the shear yielding of matrix. This phenomena is proposed by Declet-Perez *et al.*[58] as a localized network damage mechanism, which may also be in charge of the enhanced fracture toughness. It shows that debonded PIL droplets, fractured PIL droplets, voids and hyperbolic markings co-exist (Fig. 12c, c′ and d, d′), which can dissipate the energy effectively during the crack propagation.[59] Therefore, the fracture resistance of epoxy resins is effectively enhanced by the high concentrations of PIL due to the synergistic effects of multi toughening mechanisms. This is similar to systems of rubber[60] and copolymers[61] toughened epoxy.

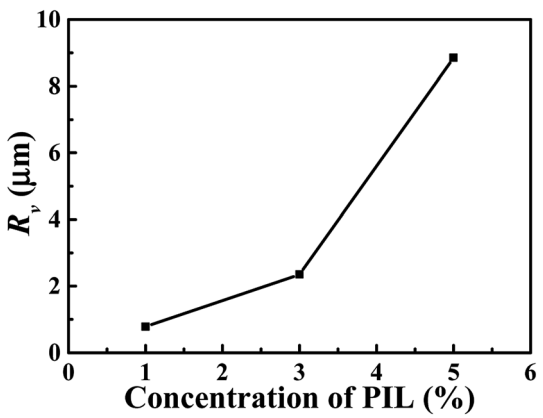

Fig. 13 The size (R_v) of PIL droplets in TDE-85/PIL composites with different concentrations (0–5 wt%) of PIL.

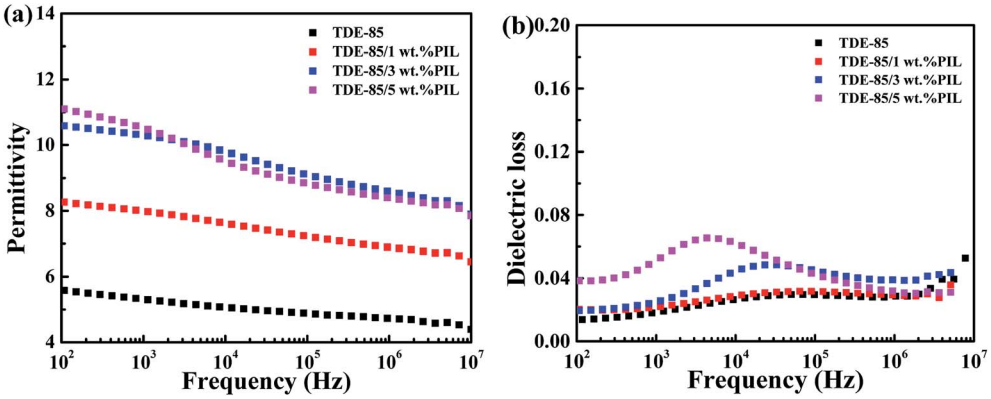

Fig. 14 Dielectric properties of TDE-85/PIL composites with the addition of different concentrations (0–5 wt%) of PIL: (a) dielectric constant *versus* frequency; (b) dielectric loss *versus* frequency.

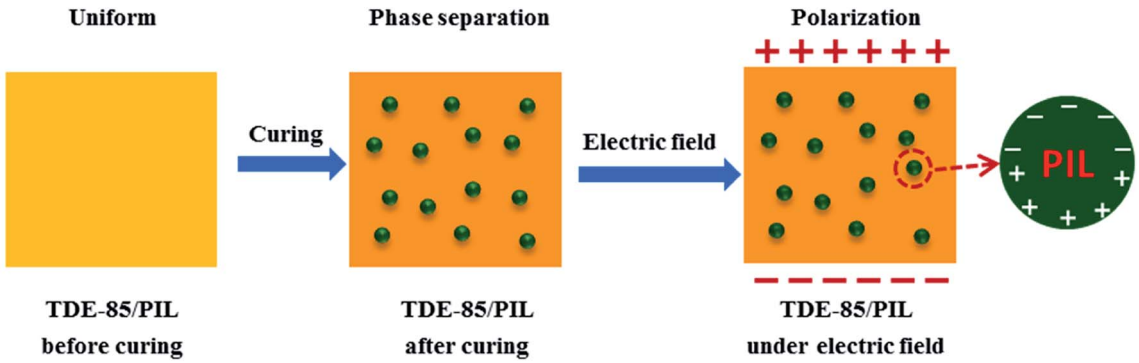

Fig. 15 Mechanism of dielectric increase of TDE-85/PIL composites under electric field.

3.5 Dielectric properties of epoxy/PIL composites

In comparison with common nonionic polymers, PIL exhibits a promising application for polymer electrolytes, whose molecules are easily polarized under electric field and possess excellent electrical properties.[23,26,31,62] Thus, effects of PIL on dielectric properties of epoxy resin are investigated. Fig. 14 shows that the dielectric properties of epoxy/PIL composites with various concentrations (0, 1, 3 and 5 wt%) of PIL. From Fig. 14a, the dielectric constant of epoxy/PIL composites in the whole frequencies is found to be markedly increased with the addition of PIL while the dielectric loss is mildly raised. Especially, at the frequency of 100 Hz, the dielectric constant is increased from 5.6 for the pure epoxy resin to 11.0 for epoxy/PIL composites with 5 wt% PIL, which is improved by 96.4%. This can be ascribed to the ionic polarization in the interior of PIL under electric field. Specifically, in the solidification process of epoxy/PIL composites, PIL is formed into microspheres through phase separation. In the PIL microspheres, it contains large amounts of cation/anion parts. Under electric field, dielectric polarizability of cation/anion parts is induced and corresponding polarization response are adequate, which makes the dielectric constant of epoxy/PIL composites increased.[63] Moreover, a conductivity is induced by the polarization of cation/anion parts due to the local movement of anions in PIL microspheres. However, the concentration of PIL is not high enough to form conductive network among PIL microspheres. Therefore, the dielectric constant of TDE-85/PIL composites is increased significantly while the dielectric loss is only increased slightly.[64] The mechanism of PIL on the dielectric properties of epoxy resins is elucidated in Fig. 15.

4. Conclusions

By adding small amounts of PIL into the multifunctional epoxy resin (TDE-85), the fracture resistance and dielectric properties of the composites are remarkably improved without sacrificing the modulus of the epoxy resin. Upon an optimal loading of 3 wt% PIL, the critical stress-intensity factor (K_{IC}) is notably raised by 92.9% meanwhile the tensile modulus and strength are raised by 13.3% and 10.7%, respectively. SEM results show that the phase separation occurs during the process of solidification of composites, forming microspheres of PIL in epoxy matrix, which answers for the improvement of the fracture resistance of composites. Moreover, with the introduction of PIL, the thermal properties of composites are significantly enhanced. When the concentration of PIL is 5 wt%, the glass transition temperature for TDE-85/PIL composites is increased by 16.58 °C, and the residual carbon weight is increased from 14.08% to 22.35% at 750 °C, which is raised by 59% in

comparison with that of pure TDE-85. In addition, the dielectric constant at low frequencies is also increased by 96.4% while the dielectric loss is slightly increased. This work will provide a strategy to obtain epoxy with relatively high toughness, thermal and dielectric properties and more types of poly(ionic liquid) are worth using to modify epoxy resin in the further.

Conflicts of interest

The authors declare no competing financial interest.

Acknowledgements

The authors are grateful for the financial support from the National Natural Science Foundation of China (51503133, 51721091), Science and Technology Department of Sichuan Province (2018GZ0458), the Programme of Introducing Talents of Discipline to Universities (B13040), and the Youth Start Funds of Sichuan University (2015SCU11030).

References

1 A. J. Kinloch, S. J. Shaw, D. A. Tod and D. L. Hunston, *Polymer*, 1983, **24**, 1341–1354.
2 A. F. Yee and R. A. Pearson, *J. Mater. Sci.*, 1986, **21**, 2462–2474.
3 S. R. Mousavi and I. A. Amraei, *J. Compos. Mater.*, 2014, **49**, 2357–2363.
4 M. Frounchi, M. Mehrabzadeh and M. Parvary, *Polym. Int.*, 2015, **49**, 163–169.
5 J. Wang, X. Zhang, L. Jiang and J. Qiao, *Prog. Polym. Sci.*, 2019, **98**, 101160.
6 R. A. Pearson and A. F. Yee, *Polymer*, 1993, **34**, 3658–3670.
7 A. J. Kinloch, M. L. Yuen and S. D. Jenkins, *J. Mater. Sci.*, 1994, **29**, 3781–3790.
8 R. D. Brooker, A. J. Kinloch and A. C. Taylor, *J. Adhes.*, 2010, **86**, 726–741.
9 Z. J. Thompson, M. A. Hillmyer, J. Liu, H. J. Sue, M. Dettloff and F. S. Bates, *Macromolecules*, 2009, **42**, 2333–2335.
10 B. Tang, M. Kong, Q. Yang, Y. Huang and G. Li, *RSC Adv.*, 2018, **8**, 17380–17388.
11 Z. Heng, X. Zhang, Y. Chen, H. Zou and M. Liang, *Chem. Eng. J.*, 2019, **360**, 542–552.
12 S. Wu, Q. Guo, M. Kraska, B. Stühn and Y.-W. Mai, *Macromolecules*, 2013, **46**, 8190–8202.
13 J. Parameswaranpillai, S. P. Ramanan, S. Jose, S. Siengchin, A. Magueresse, A. Janke and J. Pionteck, *Ind. Eng. Chem. Res.*, 2017, **56**, 14069–14077.
14 J. Parameswaranpillai, S. P. Ramanan, J. J. George, S. Jose, A. K. Zachariah, S. Siengchin, K. Yorseng, A. Janke and J. Pionteck, *Ind. Eng. Chem. Res.*, 2018, **57**, 3583–3590.
15 M. X. Li, Z. G. Heng, Y. Chen, H. W. Zou and M. Liang, *Ind. Eng. Chem. Res.*, 2018, **57**, 13036–13047.
16 B. B. Johnsen, A. J. Kinloch, R. D. Mohammed, A. C. Taylor and S. Sprenger, *Polymer*, 2007, **48**, 530–541.
17 T. H. Hsieh, A. J. Kinloch, K. Masania, A. C. Taylor and S. Sprenger, *Polymer*, 2010, **51**, 6284–6294.
18 R. D. Brooker, F. J. Guild and A. C. Taylor, *J. Mater. Sci.*, 2011, **46**, 3108–3118.
19 M. X. Zhao, M. Q. Kong, C. J. Liu, Y. J. Huang and G. X. Li, *Acta Polym. Sin.*, 2018, 721–732.
20 Y. T. Park, Y. Qian, C. Chan, T. Suh, M. G. Nejhad, C. W. Macosko and A. Stein, *Adv. Funct. Mater.*, 2015, **25**, 575–585.
21 C. R. Picu, K. K. Krawczyk, Z. Wang, H. Pishvazadeh-Moghaddam, M. Sieberer, A. Lassnig, W. Kern, A. Hadar and D. M. Constantinescu, *Compos. Sci. Technol.*, 2019, **183**, 107799.
22 H. Gu, C. Ma, J. Gu, J. Guo, X. Yan, J. Huang, Q. Zhang and Z. Guo, *J. Mater. Chem. C*, 2016, **4**, 5890–5906.
23 A. S. Shaplov, R. Marcilla and D. Mecerreyes, *Electrochim. Acta*, 2015, **175**, 18–34.
24 P. Coupillaud, J. Pinaud, N. Guidolin, J. Vignolle, M. Fèvre, E. Veaudecrenne, D. Mecerreyes and D. Taton, *J. Polym. Sci., Part A: Polym. Chem.*, 2013, **51**, 4530–4540.
25 J. Yuan and M. Antonietti, *Polymer*, 2011, **52**, 1469–1482.
26 W. Qian, J. Texter and F. Yan, *Chem. Soc. Rev.*, 2017, **46**, 1124–1159.
27 M. Kong, C. Liu, B. Tang, W. Xu, Y. Huang and G. Li, *Ind. Eng. Chem. Res.*, 2019, **58**, 8080–8089.
28 Z. Jie, X. Shen, Y. Feng, L. Qiu, S. Lee and B. Sun, *J. Mater. Chem.*, 2011, **21**, 7326–7330.
29 A. Nguyen, T. C. Rhoades, R. D. Johnson and K. M. Miller, *Macromol. Chem. Phys.*, 2017, 218.
30 K. A. Francis, C. W. Liew, S. Ramesh, K. Ramesh and S. Ramesh, *Mater. Express*, 2016, **6**, 252–258.
31 N. N. Rozik and S. L. A. El-Messieh, *Polym. Bull.*, 2017, **74**, 3595–3604.
32 T. K. Mandal, Y. Biswas, T. Maji and M. Dule, *Polym. Chem.*, 2016, **7**, 867–877.
33 Y. Ren, J. Zhang, J. Guo, F. Chen and F. Yan, *Macromol. Rapid Commun.*, 2017, **38**, 1700151.
34 J. Tang, W. Sun, H. Tang, M. Radosz and Y. Shen, *Macromolecules*, 2005, **38**, 2037–2039.
35 K. Täuber, A. Zimathies and J. Yuan, *Macromol. Rapid Commun.*, 2015, **36**, 2176–2180.
36 D. Xu, J. Guo and F. Yan, *Prog. Polym. Sci.*, 2018, **79**, 121–143.
37 W. Zhang, Q. Zhao and J. Yuan, *Angew. Chem., Int. Ed.*, 2018, **57**, 6754–6773.
38 J. Zhang, S. Chen, B. Qin, D. Zhang, P. Guo and Q. He, *Polymer*, 2019, **164**, 154–162.
39 J. Zhang, X. Mi, S. Chen, Z. Xu and D. Zhang, *J. Mol. Liq.*, 2019, **291**, 111251.
40 S. Chen, J. Zhang, J. Zhou, D. Zhang and A. Zhang, *Chem. Eng. J.*, 2018, **334**, 1371–1382.
41 M. Tunckol, E. Z. Hernandez, J.-R. Sarasua, J. Durand and P. Serp, *Eur. Polym. J.*, 2013, **49**, 3770–3777.
42 C. Xu, L. Yuan, G. Liang and A. Gu, *J. Mater. Chem. C*, 2016, **4**, 3175–3184.
43 C. Liu, P. Du, F. Nan, H. Zhao and L. Wang, *Surf. Topogr.: Metrol. Prop.*, 2018, **6**, 024004.
44 Z. Zhang, Z. Zhang, B. N. Hao, H. Zhang, M. Wang and Y. D. Liu, *J. Mater. Sci.*, 2017, **52**, 5778–5787.

45 Y. Wang, B. Song, J. Yin, Y. Zhao and Y. Sun, *Nanosci. Nanotechnol. Lett.*, 2014, **6**, 993–996.
46 T. Bing, M. Kong, Y. Qi, Y. Huang and G. Li, *RSC Adv.*, 2018, **8**, 17380–17388.
47 H. Maka, T. Spychaj, R. J. I. Pilawka and E. C. Research, *Ind. Eng. Chem. Res.*, 2012, **51**, 5197–5206.
48 M. S. Fedoseev, M. S. Gruzdev and L. F. Derzhavinskaya, *Int. J. Polym. Sci.*, 2014, **2014**, 607341–607348.
49 M. A. M. Rahmathullah, A. Jeyarajasingam, B. Merritt, M. VanLandingham, S. H. McKnight and G. R. Palmese, *Macromolecules*, 2009, **42**, 3219–3221.
50 T. K. L. Nguyen, S. Livi, B. G. Soares, S. Pruvost, J. Duchet-Rumeau and J.-F. Gérard, *ACS Sustainable Chem. Eng.*, 2015, **4**, 481–490.
51 F. C. Binks, G. Cavalli, M. Henningsen, B. J. Howlin and I. Hamerton, *Polymer*, 2018, **139**, 163–176.
52 T. Neumeyer, C. Staudigel, G. Bonotto and V. Altstaedt, *CEAS Aeronautical Journal*, 2015, **6**, 31–37.
53 H. Maka, T. Spychaj and R. Pilawka, *Ind. Eng. Chem. Res.*, 2012, **51**, 5197–5206.
54 M. W. Wang, N. I. Yu and W. H. Liao, *Adv. Mater. Res.*, 2012, **538–541**, 2224–2231.
55 K. Zhao, X.-X. Song, C.-S. Liang, J. Wang and S.-A. Xu, *Iran. Polym. J.*, 2015, **24**, 425–435.
56 B. Wetzel, P. Rosso, F. Haupert and K. Friedrich, *Eng. Fract. Mech.*, 2006, **73**, 2375–2398.
57 B. Francis, V. L. Rao, S. Jose, B. K. Catherine, R. Ramaswamy, J. Jose and S. Thomas, *J. Mater. Sci.*, 2006, **41**, 5467–5479.
58 C. Declet-Perez, E. M. Redline, L. F. Francis and F. S. Bates, *ACS Macro Lett.*, 2012, **1**, 338–342.
59 D. D. Huang, X. Feng, X. S. Du, Z. H. Lee and X. J. Wang, *J. Appl. Polym. Sci.*, 2017, **134**, 45319.
60 M. A. L. Arias, P. M. Frontini and R. J. J. Williams, *Polymer*, 2003, **44**, 1537–1546.
61 E. M. Redline, C. Declet-Perez, F. S. Bates and L. F. Francis, *Polymer*, 2014, **55**, 4172–4181.
62 D. Bondarev, J. Zedník, I. Šloufová, A. Sharf, M. Procházka, J. Pfleger and J. Vohlídal, *J. Polym. Sci., Part A: Polym. Chem.*, 2010, **48**, 3073–3081.
63 Y. Dong, J. Yin and X. Zhao, *J. Mater. Chem. A*, 2014, **2**, 9812–9819.
64 X. Zhang, L. Yuan, Q. Guan, G. Liang and A. Gu, *J. Mater. Chem. A*, 2017, **5**, 21909–21918.